Indian Journal of Fibre & Textile Research
Vol. 51, March 2026, pp. 35-45
DOI: 10.56042/ijftr.v51i1.21173

Enhanced antimicrobial and biocompatible properties of polylactic acid nanocomposites reinforced with agave sisalana cellulose nanofibres

S A Priya[1,a] & N T Nevaditha[2]

[1]Department of Chemistry & Research, Nesamony Memorial Christian College, Marthandam 629 165, India

[2]Manonmaniam Sundaranar University, Tirunelveli 627 012, India

Received 1 July 2025; revised received and accepted 7 October 2025

The growing demand for sustainable and biodegradable materials in biomedical applications motivates this study on biodegradable poly (lactic acid) (PLA) nanocomposites reinforced with cellulose nanofibres (CNFs) derived from *Agave sisalana*. The nanocomposites were fabricated via solvent casting. SEM analysis confirmed uniform dispersion of CNFs and enhanced interfacial bonding with the PLA matrix. XRD results indicated an increase in the crystalline regions of PLA due to CNF incorporation, contributing to improved mechanical strength and thermal stability, which are critical for biomedical implants. Thermal degradation studies showed a 19°C increase in degradation temperature compared to plain PLA, indicating enhanced heat resistance. Mechanical testing revealed a 48.4 % increase in tensile strength and a 66.1% increase in Young's modulus relative to plain PLA, demonstrating the reinforcing effectiveness of CNFs. Chemical degradation tests showed accelerated hydrolytic and environmental degradation of the nanocomposites compared to plain PLA, beneficial for controlled biodegradation. Additionally, antimicrobial activity improved with increasing CNF content against common pathogens. Hemolytic and MTT assays confirmed good biocompatibility at 3 wt% CNF loading, highlighting the potential of these nanocomposites for safe biomedical applications.

Keywords: Biopolymer, Cellulose, Chemical resistance, Nanocomposites, Thermal

1 Introduction

Nanocomposites are advanced materials combining nanoscale fillers with polymer matrices, offering superior properties and multifunctionality for applications like energy storage, packaging, and biomedical technologies[1]. The growing demand for sustainable and eco-friendly materials has spurred research into biopolymer-based nanocomposites, which align with the healthcare sector's emphasis on biocompatibility and biodegradability[2,3]. Poly(lactic acid) (PLA) is a biopolymer widely utilized in biomedical applications due to its tissue compatibility and biodegradability. It is extensively used in sutures, scaffolds, drug delivery systems, and implants. However, PLA's natural brittleness, low crystallinity, poor thermal stability, and moderate mechanical strength resist its use in advanced biomedical applications[4,5]. In comparison, Polyhydroxyalkanoates (PHA) offer enhanced biodegradability and mechanical properties but are expensive, while starch-based bioplastics lack the necessary mechanical and thermal resilience for biomedical use[6]. To address these limitations, researchers have incorporated natural fillers and crosslinking agents to improve PLA's mechanical, thermal, and barrier properties while preserving its biodegradability and safety for medical purposes[7].

Reinforcements such as chitosan, silk fibroin, bacterial cellulose, and hydroxyapatite have been widely studied to enhance PLA's bioactivity, mechanical integrity, and cellular response. For instance, chitosan-reinforced PLA exhibits improved antimicrobial activity and cell adhesion, while silk fibroin and collagen-based composites offer better tissue integration and flexibility[8]. Despite these advances, cellulose nanofibres (CNFs), derived from renewable sources such as plants, wood, and agricultural residues, have emerged as promising reinforcements for PLA[9,10]. Their exceptional tensile strength, high surface area, and biocompatibility make them ideal for biomedical applications like tissue scaffolds, wound dressings, and drug carriers. CNFs' hydrogen-bonded networks improve PLA's strength, toughness, and thermal stability, critical for medical devices and implants[11,12]. *Agave sisalana*, commonly

[a]Corresponding author.
E-mail: sathyarajsathya1961@gmail.com

known as sisal, has emerged as a particularly valuable source of CNFs for polymer reinforcement. Native to Mexico and cultivated in tropical and subtropical regions, Agave sisalana has traditionally been used for its durable fibres in products such as ropes and twines. Each Agave sisalana leaf contains approximately 1,000 fibres, which can be processed to extract CNFs making it an abundant and renewable source for sustainable nanocomposites[13,14]. Despite their advantages, the hydrophilic nature of CNFs poses challenges in incorporating them into the hydrophobic PLA matrix, which can hinder dispersion and interfacial bonding[15]. To overcome PLA's limitations, researchers have increasingly turned to natural fillers, bio-based plasticizers, and crosslinking strategies to tailor its physicochemical and functional characteristics without compromising its biodegradability or safety for biomedical use[16]. Eco-friendly plasticizers like triacetin and citrate esters improve PLA flexibility and processability for various applications. In addition to these conventional plasticizers, natural oils such as soybean oil, sunflower oil, and linseed oil have been explored to enhance PLA flexibility and biodegradability. Incorporating castor oil could thus provide a novel, sustainable plasticization strategy[17].

In pharmaceutical applications, Ethylene glycol dimethylacrylate (EGDMA) is valuable for creating crosslinked gels used in drug delivery systems, where it aids in the controlled release and targeting of therapeutic agents. It can be used as crosslinking agent for enhancing CNF dispersion while boosting the crystallinity, thermal stability and barrier properties of the nanocomposites[18]. These properties are vital for biomedical materials that must withstand physiological conditions and degradation timelines[19,20]. This study investigates the synthesis and characterization of PLA nanocomposites reinforced with CNFs derived from *A. sisalana*, focusing on their potential for biomedical applications. By integrating CNFs and using EGDMA, the study addresses challenges in CNF dispersion and interfacial bonding, aiming to enhance the crystallinity, thermal stability, and biodegradability of PLA.

2 Materials and Methods

2.1 Chemicals Employed

Matured leaves of *Agave sisalana* were collected from the local areas of Marthandam town, India. The chemical reagents used in this study were PolyLactic acid (PLA) (luminy175) granules were purchased from 2M biotech LLP natural works (India). Dichloromethane and Sodium hydroxide was received from Spectrochem, (Mumbai), Glacial acetic acid and Sodium chlorite was obtained from Molychem (India), Ethylene glycol dimethyl acrylate(EGDMA) was received from Sigma Aldrich. All chemicals were purchased as analytical grade and were used as received. Castor oil of poorna brand was purchased from supermarket. Distilled water was used in this study for the synthesis of CNFs.

2.2 Preparation of Cellulose Nanofibres

The thorns from mature leaves of *A. sisalana* were removed and outer layers were scraped. The fibres were cut into 3-5 cm lengths and sun-dried for three days. They were then soaked in water for two days, ground into paste, and dried into fine powder. The alkali treatment involves 5 g of fibre powder were immersed in 4 % sodium hydroxide at 75 °C for one hour to remove non-cellulosic components. Then it was washed thoroughly with distilled water to remove excess alkali and dried. After alkaline treatment the extracted cellulose was bleached with 1.5 % sodium chlorite and 1.5 % glacial acetic acid at 75 °C for 3 h. This treatment removed remaining lignin and resulted in slightly white appearance. Finally rinsed with distilled water and oven-dried at 60 °C for 2 h[21].

2.3 Preparation of Polylactic Acid Nanocomposite Films

Nanocomposite films were fabricated by dissolving 5 g of PLA pellets in 50 mL of dichloromethane, followed by the incorporation of 5 % of EGDMA as a crosslinking agent. Castor oil (10 % w/w) was added as a plasticizer. The resulting mixture was stirred thoroughly to achieve a homogeneous solution and subsequently cast into glass moulds. The films were allowed to dry at ambient conditions for 24 h. Dried films were designated as PLAF1, PLAF2, and PLAF3, corresponding to the addition of 1 wt %, 2 wt %, and 3 wt % CNFs, respectively. A control film of plain PLA was also prepared using the same procedure, excluding the CNFs. All films were carefully peeled off, oven dried at 60 °C at 1 hr and stored for further characterization.

2.4 Characterization Studies

2.4.1 Structural Analysis

FTIR spectra of the samples were recorded using Thermo Fisher Fourier Transform Infrared (FTIR) Spectrometer, equipped with Universal Attenuated Total Reflectance (ATR) accessory. The spectra were collected in the frequency range of 4,000 cm^{-1} to

600 cm^{-1}, with a spectral resolution of 4 cm^{-1}. The X-ray diffraction (XRD) pattern of the CNFs and prepared films was analyzed using a Bruker D8 Advance powder X-ray diffractometer, employing nickel-filtered Cu Kα radiation. The diffraction data were collected in the 10° to 50° 2θ range, with a scanning rate of 0.2° per minute. The morphology of CNFs and the microstructure of PLA and its nanocomposites were analyzed using a scanning electron microscope (SEM). The samples were mounted on metal stubs using double-sided tape and coated with a thin layer of gold. SEM images were captured at an accelerating voltage of 15 kV using a JEOL JSM-840 model SEM. Thermal stability was evaluated using a Shimadzu DTG 60H TGA by heating the samples from 100 °C to 800 °C under nitrogen flow of 20 mL/min.

2.4.2 Chemical Resistance Test

The degradation behaviour and solvent resistance of PLA and PLA nanocomposite films were evaluated through a chemical resistance test. All films were cut into small pieces (1 cm × 1 cm) and placed in separate beakers containing different solvent solutions of water, 5% hydrochloric acid (HCl), and 5% sodium hydroxide (NaOH) to assess the films' resistance to various solvent conditions. The films were immersed in these solvents for 72 h. After the exposure period, the films were carefully examined for signs of degradation, changes in weight, or morphological alterations. The results were tabulated, providing valuable insights into the solvent compatibility and durability of the PLA and PLA nanocomposite films.

$$Percentage\ of\ weight\ loss\ = \frac{W_{initial} - W_{final}}{W_{initial}} \times 100$$

where $W_{initial}$ and W_{final} was the weight of sample before and after treated with the chemicals.

2.4.3 Mechanical and Thermal Evaluation

Mechanical testing was done using the Instron 3345 Universal Tester equipped with 500N load cell to measure the tensile strength at the point of breakage for each sample. In accordance with ASTM D882, the films were cut into strips measuring 75mm x 10mm. A fixed crosshead speed of 10 mm/min and a gauge length of 30 mm were employed in all tests. Three specimens from each composition were tested, and the average values were calculated. Thermal stability was evaluated using a Shimadzu DTG 60H TGA by heating the samples from 100 °C to 800 °C under nitrogen flow of 20 mL/min.

2.5 Biofuntional Evaluation

2.5.1 Antimicrobial Activity

Antimicrobial activity on PLA and PLA nanocomposite films were performed against one Gram-positive bacterium (*Bacillus subtilis*), one Gram-negative bacterium (*Pseudomonas aeruginosa*), and two fungal strains (*Candida albicans* and *Aspergillus niger*) using the Kirby-Bauer disk diffusion method. The culture medium was prepared, sterilized, and supplemented with defibrinated blood when testing fastidious organisms. The medium was poured into Petri dishes and stored at +4 °C, to be used within one week. The pH of the medium was adjusted to 7.2–7.4. The bacterial inoculum was prepared by transferring the bacterial colonies to test tube containing sterile broth and incubated at 35 °C – 37 °C for 2 h to achieve a suspension with a turbidity equivalent to 0.5 McFarland units. The bacterial suspension was evenly spread over the agar surface using a sterile cotton swab. Antibiotic discs were placed on the surface using sterile forceps, ensuring even contact with the medium. The plates were incubated at 35 °C –37 °C for 16–18 h, after which the zones of inhibition were measured to the nearest millimeter using vernier calipers. The same procedure was followed for the antifungal assay. Fungal inocula were prepared similarly, and the discs were placed onto the fungal-inoculated agar surfaces. Plates were incubated at 28 °C –30 °C for 48–72 h. The results were then interpreted by comparing the measured zone sizes to standard reference tables, where the point of complete inhibition was considered as the edge of the zone.

2.5.2 Hemocompatibility Test

Human blood (5 mL) was collected from healthy volunteers into vacutainer tubes containing 3.8 % (w/v) sodium citrate to prevent coagulation. The blood was centrifuged at 1500 rpm for 5 min, and the plasma and buffy coat were carefully removed. The red blood cells (RBCs) were then washed three times with sterile 0.9 % (w/v) sodium chloride (NaCl) solution, followed by additional washes with phosphate-buffered saline (PBS, pH 7.4) to ensure purity. A 10 % RBC suspension was prepared by diluting 100 µL of packed erythrocytes in 900 µL of PBS. For the hemolysis assay, 100 µL of this suspension was incubated with 100 µL of test samples

(PLA and PLAF3) at concentrations of 10, 20, 40, 60, 80, 100, 200, 300, 400 and 500 µg/mL. PBS was used as the negative control, while 1 % (w/v) sodium dodecyl sulfate (SDS) served as the positive control. The mixtures were incubated at 37 °C for 60 minutes. After incubation, the total volume was adjusted to 300 µL with PBS, followed by centrifugation at 1500 rpm for 5 min to separate the supernatant. Hemoglobin released due to RBC lysis was quantified by measuring the absorbance at 540 nm using a UV–visible spectrophotometer. All measurements were performed in triplicate, and the percentage hemolysis was calculated using the formula:

Hemolysis (%) = Test OD/Control OD X 100 – Negative control

2.5.3 Cytocompatibility Test

The in vitro cytotoxicity of Plain PLA and PLWF3 nanocomposite samples were evaluated using Peripheral Blood Mononuclear Cells (PBMC) using the MTT assay. The cultured PBMC cells were harvested by trypsinization, collected in a 15 mL tube, and plated at a density of 1×10^5 cells/mL (200 µL per well) in a 96-well tissue culture plate. The cells were maintained in Dulbecco's Modified Eagle Medium (DMEM) supplemented with 10 % Fetal Bovine Serum (FBS) and 1 % antibiotic solution and incubated at 37 °C for 24–48 h. After incubation, the wells were washed with sterile PBS and treated with various concentrations of test samples in serum-free DMEM. Each concentration was tested in triplicate, and the cells were further incubated at 37 °C in a humidified incubator with 5 % CO_2 for 24 hours. MTT reagent (3-(4,5-Dimethylthiazol-2-yl)-2,5-diphenyltetrazolium bromide) (10 µL of 5 mg/mL) was then added to each well, and the plate was incubated for an additional 2–4 hours, allowing the formation of purple formazan crystals, which were observed under an inverted microscope. The medium containing MTT (220 µL) was aspirated, and the wells were washed with 1X PBS (200 µL). To dissolve the formazan crystals, 100 µL of DMSO was added, and the plate was gently shaken for 5 minutes. The absorbance was recorded at 570 nm using Thermo Fisher Scientific microplate reader (USA). Finally, the percentage of cell viability and IC_{50} values for the samples were determined using GraphPad Prism 6.0 software (USA).

Cell viability % = Test OD/Control OD X 100

3 Results and Discussion

3.1 FTIR Spectroscopic Analysis

The Fig. 1 presents the FTIR spectra of raw, bleached CNFs, plain PLA and PLA nanocomposite. The FTIR spectra of raw and bleached CNFs reveal key structural features related to their chemical composition. Both raw and bleached CNFs display wide prominent peak at 3412 cm^{-1}, corresponding to O-H stretching vibrations of cellulose. Peaks at 1234 cm^{-1} and 1510 cm^{-1} are associated with the aromatic skeletal vibrations of lignin, while the peak at 1730 cm^{-1} is linked to carbonyl stretching, indicating the presence of acetyl and uronic ester groups from hemicellulose as well as carboxylic groups from lignin or hemicellulose. These peaks confirm the presence of non-cellulosic components in raw CNFs but disappear in bleached CNFs, indicating the thorough cleansing of lignin and hemicellulose in bleaching[22,23]. The peak at 1163 cm^{-1} corresponds to the C–O–C asymmetric stretching of the glycosidic bond. In addition to the peak at 896 cm^{-1} is attributed to the β-1,4-glycosidic linkages, which are covalent bonds that connect glucose units in the cellulose polymer chain. In plain PLA, characteristic peaks at 1647 cm^{-1} correspond to carbonyl stretching, while peaks at 2925 cm^{-1} and 2851 cm^{-1} are related to C-H stretching vibrations of methyl and methylene groups. In PLA nanocomposites, new peaks at 950 cm^{-1} and 1165 cm^{-1} confirm the incorporation of CNFs[24]. Moreover, the slight shift and broadening of the carbonyl peak 1647 cm^{-1} in the nanocomposite compared to plain PLA suggest chemical interactions between the methacrylate carbonyl groups of EGDMA and hydroxyl groups of CNFs or terminal

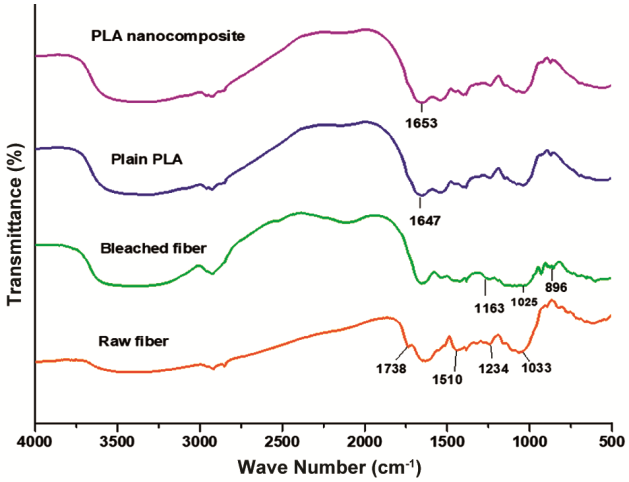

Fig. 1 — FTIR spectra of "raw fibre", "bleached fibre", plain PLA and PLA nanocomposite

PLA chains. This indicates the formation of intermolecular ester bonds via free radical polymerization, leading to a crosslinked network structure. Such crosslinking enhances interfacial adhesion between PLA and CNFs, improving the mechanical integrity and thermal stability of the composite.[25]

3.1.1 Crystallographic Analysis

The XRD analysis confirms that CNFs derived from agave fibres possess a highly crystalline structure, with a crystallinity index of 77.5 %. The distinct peaks at 21.1°, 22.2°, 26.8°, and 28.2° represent crystalline regions of cellulose II, while peaks at 22.9° and 23.8° are associated with cellulose I. The crystallinity index of the CNFs was found to be 77.5%, indicating high degree of crystallinity[26]. The CNFs have a particle size of approximately 10.5 nm, calculated using the Scherrer equation. The Fig. 2. shows the XRD pattens of CNF, plain PLA and PLA nancomposites. The Plain PLA exhibits characteristic semicrystalline peaks at 16.6°, 19.1°, and 22.5°. These new peaks, along with a shift in PLA's characteristic peaks from 16.6° to 17.7° and 19.1° to 20.4°, indicate proper dispersion and interaction of CNFs within the PLA matrix, enhancing the nanocomposite's crystallinity and overall structural properties. The minor differences in peak intensity and shape across the PLA nanocomposites indeed suggest varying degrees of crystallinity and phase interactions due to the levels of CNF loading. Therefore, the presence of CNFs at different concentrations impacts the extent of crystallization in PLA, leading to the formation of more nucleation sites and enhancing the crystallinity of the PLA nanocomposites[27].

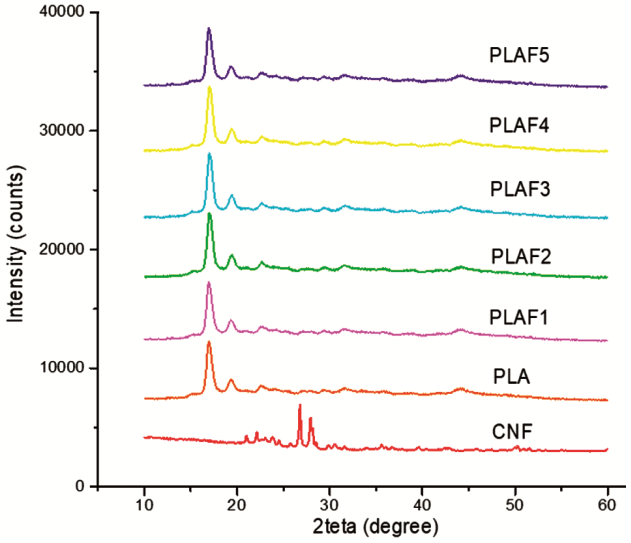

Fig. 2 — XRD patterns of CNFs, plain PLA and PLA nanocomposites

3.1.2 Surface Topographical Analysis

The SEM analysis compares the surface morphologies of untreated CNFs, treated CNFs, plain PLA, and PLA based nanocomposite films (PLAF2). Figure 3(a) displays the untreated CNFs have more rugged structure with fibre bundles due to non-cellulosic components like lignin and hemicellulose. After mercerization and bleaching, treated CNFs exhibit well-separated, uniform fibrils with flattened surfaces which indicates successful purification and nanoscale fibrillation as shown in Fig. 3 (b). The plain PLA film displays smooth, homogeneous surfaces with effective film formation (Fig. 3(c). In contrast, Fig. 3(d) shows that the PLA nanocomposite has a rough surface without fractures, indicating strong adhesion between the PLA matrix and embedded CNFs, with even CNFs dispersion. These interactions contribute to enhanced crystallinity and thermal resistance in the nanocomposite[28,29]**.** Fig. 3(e), reveals that CNFs are moderately dispersed within the matrix, exhibiting localized regions of agglomeration and clustering, along with the presence of microvoids.

3.1.3 Chemical Degradation Studies

The chemical resistance test results are shown in Fig. 4, illustrating the impact of CNF incorporation on the degradation behaviour of PLA under different conditions: 5 % NaOH, 5 % HCl, and water. In alkaline conditions (5 % NaOH), all samples began to degrade after six hours. Plain PLA exhibited a weight loss of 15.1 %, which increased with CNF content to 21.2 % for PLAF1, 28.5 % for PLAF2, 35.2 % for PLAF3, 39.6 % for PLAF4, and 47.3 % for PLAF5. This indicates that CNFs enhance the hydrophilicity of the nanocomposites, increasing susceptibility to alkaline hydrolysis, where NaOH cleaves the ester bonds in PLA and accelerates degradation. In acidic conditions (5 % HCl), degradation was lower, and swelling was observed after 24 h. The weight loss for plain PLA was 10 %, while PLAF1, PLAF2, PLAF3, PLAF4, and PLAF5 exhibited 12.0 %, 16.2 %, 20.4 %, 24.3 %, and 28.6 %, respectively. This suggests that plain PLA is relatively acid-resistant, but the presence of CNFs introduces more hydroxyl groups, facilitating acid penetration and accelerating degradation. In water, plain PLA showed minimal

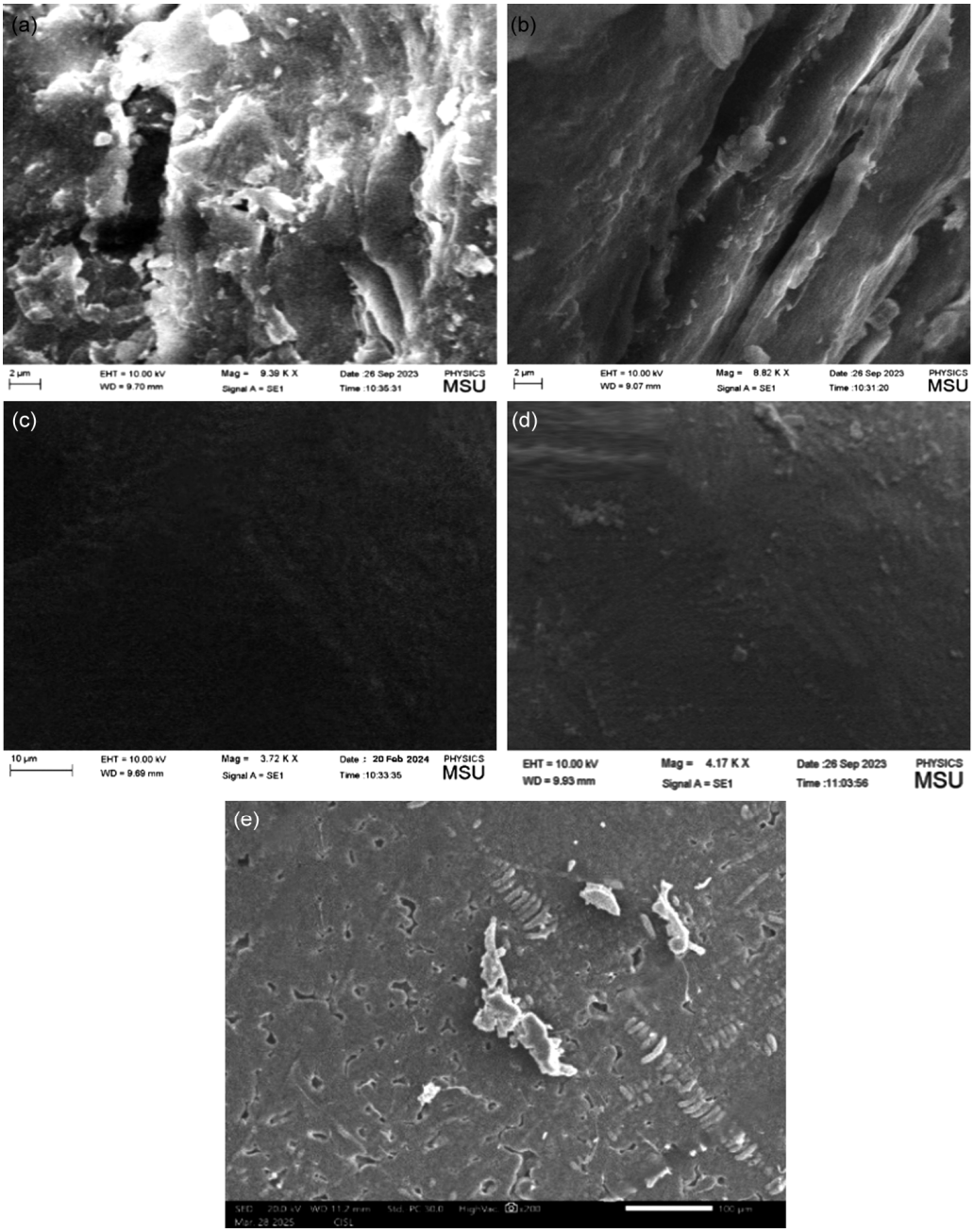

Fig. 3 — SEM images of (a) "raw fibres" (b) "bleached fibres" (c) plain PLA (d) PLAF2 (e) PLAF4

weight loss of 2.5 %, indicating low hydrolytic degradation, but with increasing CNF content, weight loss rose to 4% for PLAF1, 9.8 % for PLAF2, 12.4 % for PLAF3, 15.5 % for PLAF4, and 18.3 % for PLAF5. The increased water absorption is attributed to the hydrophilic nature of CNFs, which retain moisture and promote hydrolytic chain scission in PLA. Although physiological fluids such as blood plasma, interstitial fluid, or simulated body fluids (SBF) are buffered near neutral pH (7.35–7.45), local inflammation or pathological conditions may transiently shift pH, potentially accelerating degradation[30].

3.1.4 Thermal Stability Analysis

Thermo gravimetric Analysis (TGA) of plain PLA and PLA nanocomposites typically reveals two distinct regions of weight loss, as illustrated in

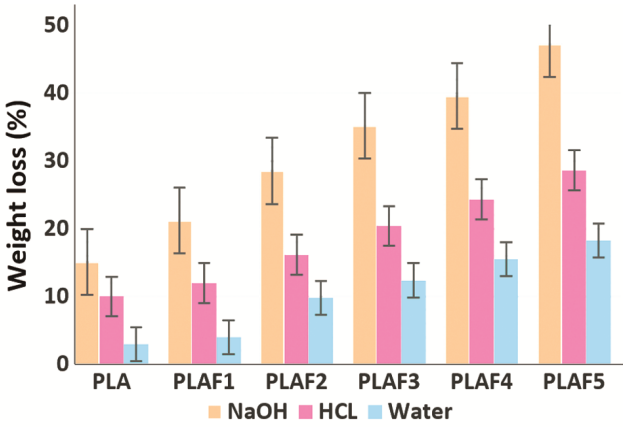

Fig. 4 — Bar chart of percentage of weight loss in plain PLA and PLA nanocomposites

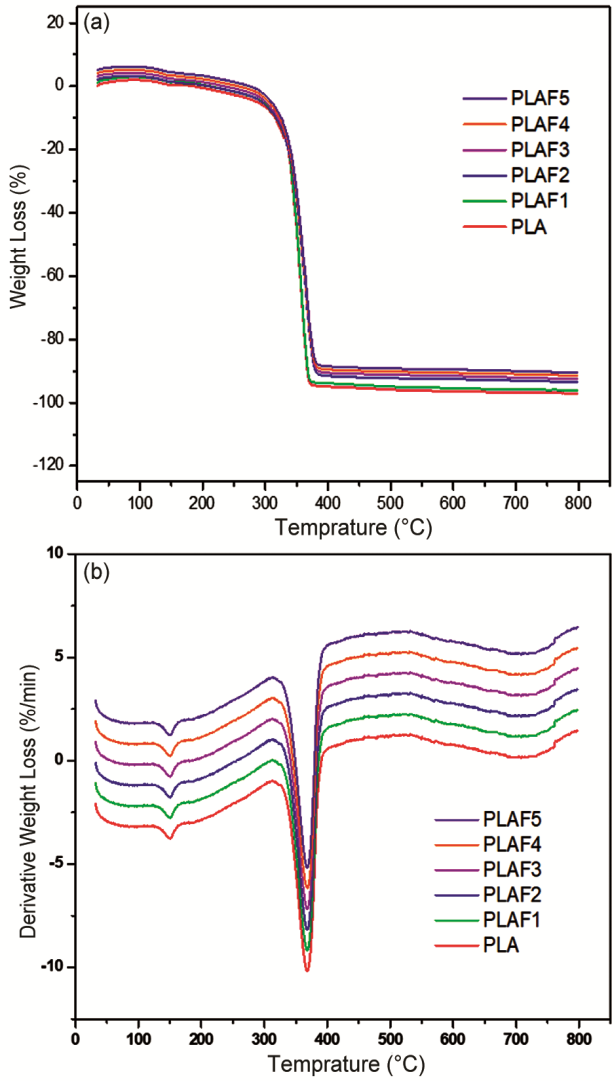

Fig. 5 — (a) Thermo gravimetric curves (TGA), and (b) Differential thermos gravimetric (DTA) curves of plain PLA and PLA nanocomposites

Table 1 — TGA data of plain PLA and PLA nanocomposites

Samples	T_{onset}, ˚C	$T_{50\%}$, ˚C	T_{max}, ˚C	Residue, %
PLA	146.94	343.92	351.94	1.676
PLAF1	152.12	346.68	356.84	1.738
PLAF2	154.25	349.48	359.99	1.836
PLAF3	157.13	352.56	364.60	1.973
PLAF4	159.21	361.73	367.45	2.673
PLAF5	160.34	364.12	371.62	3.215

Table 1 and Fig 5(a) and (b). The first region, observed approximately at 150 °C, represents the evaporation of moisture contained in the nanocomposites, contributing to a weight loss of around 5 %. The second region, occurring between 250 °C and 360 °C, exhibits significant weight loss of about 75 %, primarily due to the degradation of cellulose and the polymer's main structural components. Beyond 400 °C, weight loss continues as char residues undergo combustion, resulting in a further reduction in weight[31]. The Differential Thermo gravimetric Analysis (DTA) curves show a shift in the degradation temperature from 350 °C (for plain PLA) to 370 °C (for PLA nanocomposites), indicating enhanced thermal stability in the nanocomposites. This shift suggests that the incorporation of CNFs, which increase the crystallinity of the polymer matrix, improves the composite's overall thermal resistance. Additionally, the presence of CNFs in the PLA matrix not only enhances thermal stability but also influences the degradation profile by restricting polymer chain mobility, thereby delaying thermal decomposition. The improved thermal stability of PLA nanocomposites can be attributed to the strong interfacial interactions between CNFs and the PLA matrix, which act as a thermal barrier, suppressing the mobility of polymer chains and reducing heat transfer. Moreover, CNFs decompose at higher temperatures compared to PLA, contributing to a more stable degradation process. The increased residual mass observed at elevated temperatures further confirms the reinforcing effect of CNFs, as they promote char formation, reducing overall mass loss and improving heat resistance[32].

3.1.5 Mechanical Properties

The tensile strength and Young's modulus of PLA and its nanocomposites exhibit a marked improvement with increasing CNF content. Figure 6(a) to (c) presents the mechanical properties of plain PLA and its nanocomposites. The plain PLA shows a

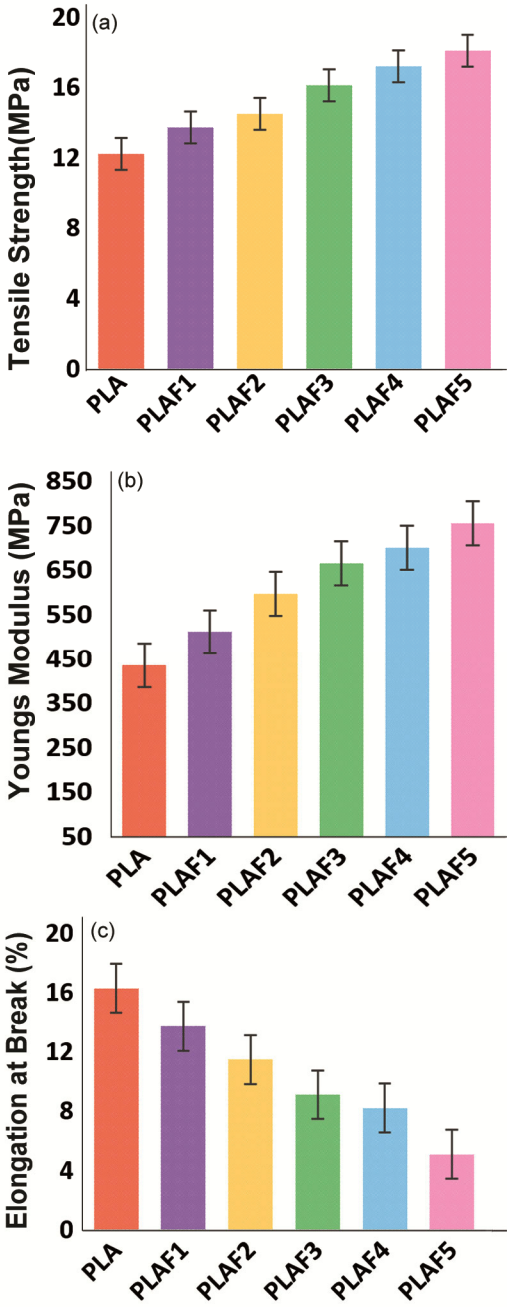

Fig. 6 — Mechanical properties of plain PLA and PLA nanocomposites: (a) tensile strength, (b) young modulus, and c) elongation at break

tensile strength of 12.24 ± 1.22MPa and a Young's modulus of 456 ± 1.31 MPa, reflecting its relatively low mechanical performance. The addition of CNFs increases the tensile strength to 18.12 ± 1.54 MPa and Young's modulus reaches 757± 1.43MPa, indicating enhanced stiffness and load-bearing capacity as a result of effective CNFs reinforcement. This enhancement is attributed to the high aspect ratio and surface functionality of CNFs, which promote strong hydrogen bonding interactions with PLA chains, enhancing interfacial adhesion and enabling efficient stress transfer between the matrix and the reinforcing phase[33]. Consistent with our results, previous studies have shown that cellulose nanocrystals (CNCs) extracted from oil palm mesocarp fibre and kenaf bast fibres have demonstrated improvements in tensile strength and thermal stability of PLA composites, although surface modification is often necessary to achieve optimal dispersion and interfacial bonding[33,34]. Moreover, CNFs act as nucleating agents, promoting increased crystallinity within the PLA structure. The resulting more organized and rigid polymer morphology contributes to enhanced dimensional stability and mechanical rigidity under applied stress[35]. However, CNF addition substantially reduced elongation at break 62 % indicating decreased ductility. This reduction is linked to the rigid, reinforcing nature of CNFs, which restrict plastic deformation, and is further exacerbated by EGDMA crosslinking that forms a constrained polymer network. Although castor oil (10 wt %) was incorporated as a plasticizer, its effect was insufficient to counteract the stiffening induced by CNFs and crosslinking. In addition, poor filler dispersion or suboptimal interfacial adhesion may promote early crack initiation at the filler–matrix interface, further contributing to brittleness[36,37].

3.2 Biological Studies

3.2.1 Antimicrobial Activity

Figures 7(a) to (d) show the antimicrobial efficacy of plain PLA and its nanocomposite films reinforced with increasing concentrations of CNFs was systematically investigated against both fungal and bacterial pathogens. The antibacterial activity was first assessed against *Bacillus subtilis* and *Pseudomonas aeruginosa*. Plain PLA exhibited modest inhibition, producing zones of 12 mm and 9 mm, respectively. However, with the progressive incorporation of CNFs, the antimicrobial performance significantly improved. The addition of 1 wt % CNF resulted in inhibition zones of 11 mm for *B. subtilis* and 13.7 mm for *P. aeruginosa*. A further increase in CNF content led to a substantial enhancement in antibacterial activity, with the nanocomposite film containing 5 wt % CNFs achieving inhibition zones of 18.1 mm and 18.8 mm against *B. subtilis* and *P. aeruginosa*, respectively. These values surpass

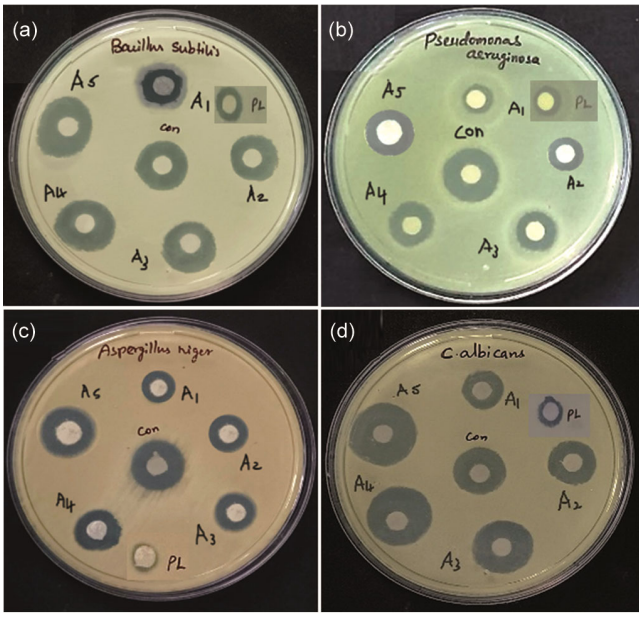

Fig. 7 — Antimicrobial activity of plain PLA and PLA nanocomposites: (a) Bacillus subtilis, (b) Pseudomonas aeruginosa, (c) Candida albicans, and (d) Aspergillus niger

Fig. 8 — Hemolysis assay of PLAF3 nanocomposite at various concentrations (10–500 µg/mL). NC = Negative control (PBS); PC = Positive control (1% SDS).

the inhibition zones of the control (Amikacin 17 mm), indicating potent antibacterial activity of the nano composites. In terms of antifungal activity, plain PLA exhibited relatively low inhibition against *Candida albicans* and *Aspergillus niger*, with zones of 10 mm and 7 mm, respectively. The addition of CNFs markedly improved antifungal efficacy, with PLAF5 achieving inhibition zones of 16.6 mm against *C. albicans* and 16.2 mm against *A. niger*, which are comparable to those of the reference (Nystatin 17 mm). These findings confirm that the incorporation of CNFs into the PLA matrix significantly enhances its antimicrobial properties, making the nanocomposite films promising candidates for biomedical applications where microbial resistance is essential[37]. Similarly, chitosan, a biopolymer with inherent antimicrobial properties, has been used to reinforce PLA, enhancing biocompatibility and antimicrobial activity[38].

Table 2 — Hemolysis effect of plain PLA and PLNF3 on human red blood cells

Concentration, µg/ml	Hemolysis, %	
	Plain PLA	PLAF3
Positive control	100	100
Negative control	0	0
500 (µg/ml)	5.21 ± 1.34	4.15± 1.13
400 (µg/ml)	2.66 ± 0.23	2.91± 0.13
300 (µg/ml)	0.12 ± 0.04	0.87±0.32
200 (µg/ml)	0	0.32±0.03
100 (µg/ml)	0	0

3.2.2 Hemolytic Assessment of PLAF3

In this study, hemocompatibility testing was performed exclusively on the PLAF3 nanocomposite film, identified as the optimal formulation based on its structural, mechanical, thermal, and antimicrobial performance. This selective assessment aimed to preliminarily evaluate the nanocomposite's suitability for biomedical applications. However, comprehensive biocompatibility profiling across all filler loadings (1–5 wt%) is recommended to establish dose-dependent biological responses. The hemolytic response of plain PLA and its nanocomposite formulation (PLAF3) was systematically assessed over a concentration range of 100–500 µg/mL to evaluate their blood compatibility. As shown in Table 2 and Fig 8, PLAF3 consistently exhibited lower hemolysis percentages than plain PLA across all tested concentrations, indicating improved erythrocyte compatibility. At the highest concentration of 500 µg/mL, plain PLA induced a hemolysis rate of 5.21 ± 1.34 %, classifying it as hemolytic according to ISO 10993-4 standards (>5%). In contrast, PLAF3 demonstrated a significantly reduced hemolysis of 4.15±1.13%, falling within the slightly hemolytic range (2–5 %). A concentration-dependent decline in hemolytic activity was observed for both materials. However, PLAF3 maintained a consistently lower hemolytic profile. At 300 µg/mL and below, hemolysis was negligible for both samples, with values approaching zero, and no hemolytic activity was detected at 100 µg/mL. The superior hemocompatibility of PLAF3 relative to plain PLA is attributable to the presence of CNFs, which is likely to alter surface topography, increase hydrophilicity, and reduce interfacial tension, thereby mitigating erythrocyte membrane disruption[39,40].

3.2.3 Cytotoxicity Studies

The in vitro cytotoxicity of plain PLA and the PLAF3 nanocomposite was assessed using the MTT

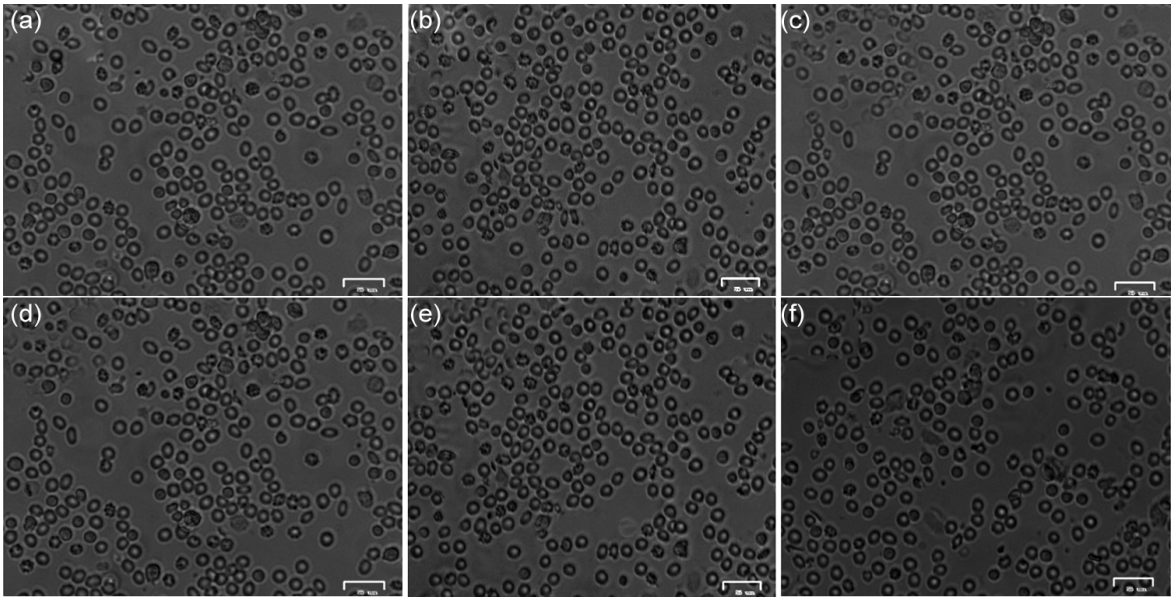

Fig. 9 — Cell viability of PLAF3 at varying Concentrations: (a) control, (b) 400µg/mL, (c) 200µg/mL, (d) 80µg/mL, (e) 40 µg/mL, and (f) 10µg/mL

assay in human cell lines across a concentration range of 10–500 µg/mL. The cytotoxicity response of PLAF3 at different concentrations on PBMCs is presented in Fig. 9. The percentage of viable cells was determined relative to the untreated control group, which was set at 100 % viability. At the highest concentration tested (500 µg/mL), PLA exhibited a cell viability of 69.75 %, while PLAF3 showed a slightly lower value of 72.25 %. At an intermediate concentration (100 µg/mL), PLAF3 maintained cell viability exceeding the ISO 10993-5 standard threshold for non-cytotoxic materials (>70 %). At lower concentrations (80 -10µg/mL), PLAF3 showed excellent cytocompatibility, with viability values increasing from 84.55 to 94.52 %, closely approaching plain PLA, which ranged from 82.33 % to 92.38 % within the same concentration range. However, as the concentration decreased, a progressive improvement in cell viability was observed for both materials. These results indicate that incorporating CNFs into PLA does not significantly compromise cytocompatibility[41,42].

4 Conclusion

This study demonstrates the potential of Agave sisalana cellulose nanofibres (CNFs) as effective reinforcements for polylactic acid (PLA), enhancing crystallinity, thermal stability, mechanical strength, and structural integrity. Chemical degradation tests revealed accelerated breakdown under acidic and alkaline conditions, indicating reduced stability in physiological environments and necessitating further evaluation for long-term biomedical use. Surface modifications such as hydrophobic coatings, plasma treatment, or crosslinking with citric acid or genipic acid may improve hydrolytic stability without compromising biocompatibility. Thermogravimetric analysis showed improved thermal stability up to 371 °C compared to plain PLA. Although increased brittleness (62 %) may limit load-bearing applications, it can be advantageous in temporary implants, wound healing, or drug delivery systems where short-term mechanical integrity is sufficient. Future work should investigate ductile biopolymers or bio-based plasticizers to enhance flexibility while preserving biodegradability. The antimicrobial activity of the nanocomposites was improved due to the presence of CNFs against both bacterial and fungal strains. Hemolytic analysis at optimized CNF loadings supports the safety of these nanocomposites for biomedical applications. Cytotoxicity studies further confirm their good cytocompatibility. These results highlight the promise of these materials for short-term or resorbable uses.

References

1 Bikiaris N D, Koumentakou I, Samiotaki C, Meimaroglou D, Varytimidou D, Karatza A, Kalantzis Z, Roussou M, Bikiaris R D & Papageorgiou G Z, *Polymers*, 15 (5) (2023) 1196.

2 Monfared A R, Omranpour H, Tuccitto A V, Zaoui A, Rahman S S, Kheradmandkeysomi M, Jalali A & Park C B, *ACS Sust Chem Eng*, 12 (34) (2024) 13017.

3 Patra N, Gopi V S & Brahman P K, In: Kesari K K, Prakash C, Khalid M & Negi A (eds), *Functionalized Cellulose Materials, Springer, Cham*, (2025).

4 Shalan A E, Makhlouf A S H & Lanceros-Méndez S, *Adv Nanocompos Mater Environ Energy*, 3 (2022) 14.

5 Udayakumar G P, Muthusamy S, Selvaganesh B, Sivarajasekar N, Rambabu K & Banat F, J *Environ Chem Eng*, 9 (2021) 105322.

6 Jem K J & Tan B, *Adv Ind Eng Polym Res*, 3 (2) (2020) 60.

7 Klemm D, Heublein B, Fink H P & Bohn A, *Angew Chem Int Ed*, 44 (22) (2005) 3358.

8 Khouri N G, Bahú J O, Blanco-Llamero C, Severino P, Concha V O & Souto E B, *J Mol Struct*, 1309 (2024) 138243.

9 Chieng B W, Lee S H, Ibrahim N A, Then Y Y & Loo Y Y, Polymers, 9 (8) (2017) 355.

10 Kargarzadeh H, Ahmad I, Abdullah I, Dufresne A, Zainudin S Y & Sheltami R M, *Cellulose*, 19 (3) (2012) 855.

11 Agbakoba V C, Mokhena T C, Ferg E E, Hlangothi S P & John M J, *Cellulose*, 30 (2023) 11537.

12 Patra N, Gopi V S & Brahman P K, In: Kesari K K, Prakash C, Khalid M & Negi A (eds), Functionalized Cellulose Materials, Springer, Cham, (2025) ch 8.

13 Stella S M, Sridhar T M, Ramprasath R, Gimbun J & Vijayalakshmi U, *Polymers*, 15 (1) (2023) 155.

14 Credou J & Berthelot T, *J Mater Chem B*, 2 (30) (2014) 4767.

15 Eichhorn S J, Dufresne A, Aranguren M, et al., *J Mater Sci*, 36 (2009) 2107.

16 Lomelí-Ramírez M G, Reyes-Alfaro B, Martínez-Salcedo S L, González-Pérez M M, Gallardo-Sánchez M A, Landázuri-Gómez G, Vargas-Radillo J J, Diaz-Vidal T, Torres-Rendón J G, Macias-Balleza E R & García-Enriquez S, *Polymers*, 15 (18) (2023) 3793.

17 Tingaut P, Zimmermann T & Lopez-Suevos F, *Biomacromolecules*, 11 (2) (2010) 454.

18 Paul U C, Fragouli D, Bayer I S, Zych A & Athanassiou A, *ACS Appl Polym Mater*, 3 (6) (2021) 3071.

19 Shaipulizan N S, Md Jamil S N A, Kamaruzaman S, Subri N N S, Adeyi A A, Abdullah A H & Abdullah L C, *Polymers*, 12 (2) (2020) 423.

20 Zhou L, Ke K, Yang M B & Yang W, *Compos Commun*, 23 (2021) 100548.

21 Akhtar M F, Ranjha N M & Hanif M, *J Pharm Biomed Anal*, 23 (1) (2015) 41.

22 Simmons H, Tiwary P, Colwell J E & Kontopoulou M, *Polym Degrad Stab*, 166 (2019) 248.

23 Kavkler N, Gunde-Cimerman P, Zalar A & Demšar A, *Polym Degrad Stab*, 96 (4) (2011) 574.

24 Shojaeiarani J, Bajwa D S & Hartman K, *Cellulose*, 26 (4) (2019) 2349.

25 Rahman M M, Afrin S, Haque P, Islam M M, Islam M S & Gafur M A, *Int J Chem Eng*, 2014 (2014) 842147.

26 Zaini L H, Jonoobi M, Tahir P M & Karimi S, *J Biomater Nanobiotechnol*, 4 (2013) 37.

27 Yasuniwa M, Tsubakihara S, Iura K, Ono Y, Dan Y & Takahashi K, *Polymer*, 47 (21) (2006) 7554.

28 Noh S, Sung H, Kim J R, Lee E, Yoon K C, Kim J & Ku S H, *J Polym Res*, 31 (2024) 355.

29 Fardioui M, Stambouli A, Gueddira T, Dahrouch A, Qaiss A E K & Bouhfid R, *J Polym Environ*, 24 (4) (2016) 356.

30 Hwang U, Moon H, Park J & Jung H W, *Polymers*, 16 (15) (2024) 2149.

31 Sleinus D, Lovato M J, Platnieks O, Sabalina A, Gaidukovs S, Franco L, Puiggalí J & del Valle L J, *RSC Adv*, 15 (9) (2025) 6753.

32 Uribe-Calderón J, Rodrigue D, Hirschberg V, Fernández-Escamilla V V & Pech-Cohuo S C, *Polym Bull*, 80 (9) (2023) 10193.

33 Clarkson C M, El Awad Azrak S M, Chowdhury R, Shuvo S N, Snyder J & Schueneman G, *ACS Appl Polym Mater*, 1 (2) (2018) 160.

34 Asyraf M R M, Ishak M R, Syamsir A, Nurazzi N M, Sabaruddin F A, Shazleen S S, Norrrahim M N F, Rafidah M, Ilyas R A, Rashid M Z A & Razman M R, J Mater Res Technol, 17 (2022) 33.

35 Aumnate C, Soatthiyanon N, Makmoon T & Potiyaraj P, Cellulose, 28 (2021) 8509.

36 Hui I, Pasquier E, Solberg A, Agrenius K, Håkansson J & Chinga-Carrasco G, J Mech Behav Biomed Mater, 147 (2023) 106136.

37 Dong J, Li M, Zhou L L, Lee S Y, Mei C, Xu X & Wu Q, *J Polym Sci B Polym Phys*, 55 (11) (2017) 847.

38 Liu H Y, Du L, Zhao Y T & Tian W Q, *J Nanomater*, 2015 (2015) 685323.

39 Jerlite K J J & Nevaditha N T, *Int J Health Sci*, 6 (S2) (2022) 5613.

40 Yu H, Li Y, Pan Y, Wang H, Wang W, Ren X, Yuan H, Lv Z, Zuo Y, Liu Z, Lin W & Yao Q, J *Nanobiotechnol*, 21 (1) (2023) 110.

41 Yang Z, Si J, Cui Z, Ye J, Wang X, Wang Q, Peng K, Chen W & Chen S C, *Carbohydr Polym*, 174 (2017) 750.

42 Zhang Y, Jiang S, Xu D, Li Z, Guo J, Li Z & Cheng G, *Polymers*, 15 (10) (2023) 2323.